

No Nematicity at the Onset Temperature of the Pseudogap Phase in the Cuprate Superconductor $\text{YBa}_2\text{Cu}_3\text{O}_y$

G. Grissonnanche^{1,2,3,*}, O. Cyr-Choinière¹, J. Day⁴, R. Liang⁴, D. A. Bonn⁴, W. N. Hardy⁴,
N. Doiron-Leyraud¹ and L. Taillefer^{1,5,†}

¹*Institut quantique, Département de physique and RQMP, Université de Sherbrooke, Sherbrooke, Québec J1K 2R1, Canada*

²*Laboratory of Atomic and Solid State Physics, Cornell University, Ithaca, New York 14853, USA*

³*Kavli Institute at Cornell for Nanoscale Science, Ithaca, New York 14853, USA*

⁴*Department of Physics and Astronomy, University of British Columbia, Vancouver, British Columbia V6T 1Z1, Canada*

⁵*Canadian Institute for Advanced Research, Toronto, Ontario M5G 1M1, Canada*

 (Received 11 May 2022; revised 25 May 2023; accepted 9 June 2023; published 25 July 2023)

Electronic nematicity is the spontaneous loss of rotational symmetry in a metal, without breaking translational symmetry. In the cuprate superconductors, there is experimental evidence for nematicity, but its origin remains unclear. Here we investigate the onset of nematicity in the transport of charge by means of electric and thermoelectric measurements in underdoped $\text{YBa}_2\text{Cu}_3\text{O}_y$, performed by passing the current (electrical or thermal) first along the a axis then the b axis of the orthorhombic structure in the same crystal, with a hole doping $p = 0.12$. Upon cooling, we observe no additional in-plane anisotropy—beyond the background anisotropy due to the CuO chains—in either the resistivity ρ or the Seebeck coefficient S as the temperature T^* for the onset of the pseudogap phase is crossed. We conclude that the pseudogap phase of cuprates is not nematic. However, at temperatures much lower than T^* , a strong additional anisotropy is observed, most clearly in the Peltier coefficient $\alpha = S/\rho$. We interpret it as nematicity associated with the development of charge order.

DOI: [10.1103/PhysRevX.13.031010](https://doi.org/10.1103/PhysRevX.13.031010)

Subject Areas: Condensed Matter Physics,
Strongly Correlated Materials,
Superconductivity

I. INTRODUCTION

The way in which strong electronic correlations give rise to high temperature superconductivity remains a mystery. Hole-doped cuprates possess the highest superconducting transition temperatures of all unconventional superconductors. In these quantum materials, superconductivity coexists with the pseudogap phase—one of the most studied enigmas of strongly correlated materials for the role it might play in the mechanism of electron pairing [1,2].

The pseudogap phase appears below a temperature T^* (defined by a change in either the electrical resistivity or the Nernst coefficient [3]) that ends inside the superconducting dome [Fig. 1(a)]. Among the many reports of broken

symmetries below T^* [4–7], the loss of rotational symmetry without breaking translational symmetry—known as nematicity—has been a recurring theme not only in cuprates but also in other unconventional superconductors [8–10], with an unequivocal demonstration in iron pnictide superconductors based on the anisotropy of the resistivity [9].

In cuprates, there is strong evidence of nematicity deep inside the pseudogap phase [13–15], and some studies—based on Nernst [16], magnetic torque [11], and elastoresistance [17] measurements—report the onset of nematicity at T^* (Fig. 1). These studies indicate that the pseudogap phase is inherently nematic, which in turn suggests that nematicity may play a role in boosting superconductivity [18,19].

In the cuprate $\text{YBa}_2\text{Cu}_3\text{O}_y$ (YBCO), magnetic torque experiments [11] report the sudden onset of broken rotational symmetry at a temperature T_χ that coincides with T^* [Fig. 1(b)], but it is unclear whether this nematicity is a property of the electron fluid. Nernst experiments [16] show the gradual onset of an additional anisotropy—between the a and b crystallographic directions of the orthorhombic crystal structure—at a temperature T_ν that also coincides with T^* . This points toward the onset of

*gael.grissonnanche@cornell.edu

†louis.taillefer@usherbrooke.ca

Published by the American Physical Society under the terms of the [Creative Commons Attribution 4.0 International license](https://creativecommons.org/licenses/by/4.0/). Further distribution of this work must maintain attribution to the author(s) and the published article's title, journal citation, and DOI.

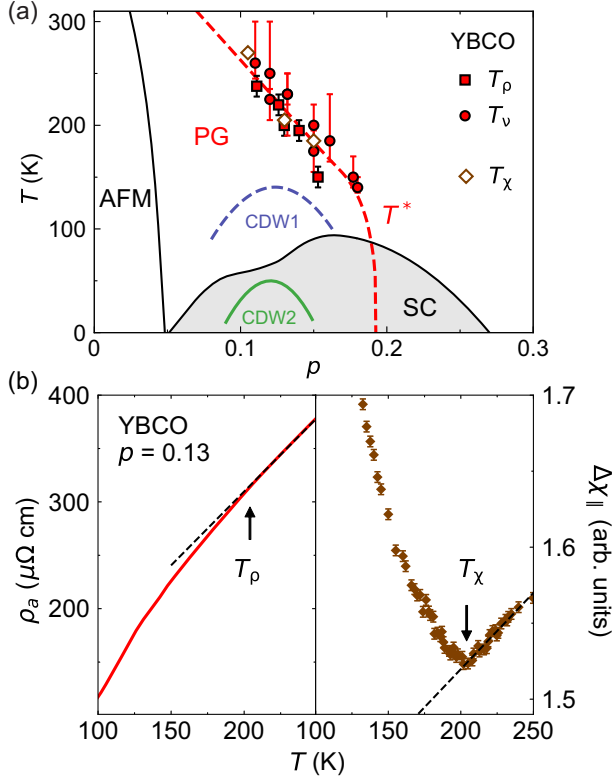


FIG. 1. (a) Temperature versus doping phase diagram of YBCO, showing the antiferromagnetic (AFM) phase, the dome of superconductivity (SC), and the pseudogap phase (PG), as well as the regions of short-range charge-density-wave correlations (CDW1) and long-range charge order (CDW2). The red dashed line marks T^* , the onset temperature of the pseudogap phase, defined by the drop in either the resistivity (T_ρ , full red squares) or the Nernst coefficient (T_ν , full red circles) [3]. T_χ marks the onset of anisotropy in torque measurements (open brown diamonds [11]). (b) Left: temperature dependence of the a -axis resistivity of YBCO at $p = 0.13$ [12]. The deviation from T -linear resistivity (dashed line) below T_ρ defines T^* . Right: in-plane anisotropy of the magnetic susceptibility χ , plotted as $\Delta\chi_{\parallel}$ versus T , as measured by torque on YBCO at $p = 0.13$ [11]. T_χ marks a sharp signature in the data, found to coincide with T^* .

nematicity, at T^* , in the electron fluid that flows in the CuO_2 planes. However, the Nernst coefficient ν is a composite of four electric and thermoelectric, longitudinal and transverse, transport coefficients:

$$\nu_i = R_H \alpha_i - \frac{\alpha_{ij} \rho_i}{B}, \quad (1)$$

where ν_i is the Nernst coefficient for a current along the i direction ($i, j = a$ or b), R_H is the Hall coefficient, α_i and α_{ij} are the longitudinal and transverse Peltier coefficients, and ρ_i is the resistivity. This makes the Nernst coefficient difficult to interpret, since a change in any of the four constituent coefficients can create a collateral anisotropy between ν_a and ν_b that would not be an expression of

nematicity. This calls for the measurement of a pure longitudinal transport coefficient in order to settle the existence of nematicity occurring at T^* .

In this article, we investigate the nematicity in the charge transport properties of YBCO, at a hole doping $p = 0.12$. At this doping, the pseudogap temperature is $T^* = 220 \pm 10$ K [12], the short-range charge-density-wave correlations (CDW1) onset at $T_{\text{CDW1}} = 140 \pm 10$ K [20], and the charge-density-wave order becomes long-range (in a field larger than $H = 15$ T) and unidirectional below $T_{\text{CDW2}} = 47 \pm 1$ K [21] [Fig. 1(a)].

To reliably measure the transport anisotropy between the a and b directions of the orthorhombic structure in YBCO, the longitudinal electric and thermoelectric transport coefficients—the resistivity ρ and the Seebeck coefficient S —were measured on the same sample with the same contacts, before and after inverting the a and b directions in the single crystal. Following this method, we detect no additional anisotropy in either transport coefficient upon cooling through T^* . As we explain below, the onset of nematicity at T^* reported previously from Nernst measurements is an artifact of the composite nature of that transport coefficient. We conclude that the pseudogap phase is not inherently nematic in its metallic properties. However, at this doping, there is indeed a strong nematicity that emerges deep inside the pseudogap phase, in tandem with the development of charge order at low temperature.

II. METHODS

A. Material

To study nematicity in a tetragonal crystal, fourfold rotational symmetry must ideally be broken on a macroscopic scale in order for any nematic domains, if present, to all be aligned. This is the necessary condition for a nematic monodomain to form and be amenable to transport anisotropy studies. One way to achieve this is to apply uniaxial pressure to force domains to align in one direction, as done in iron pnictides [9]. The cuprate material YBCO has been a favorite playground for the study of nematicity because its orthorhombic structure will naturally align nematic domains. Indeed, by detwinning a single crystal of YBCO, so that it becomes a single structural monodomain, the entire sample hosts a preferential direction. In other words, the orthorhombic structure then becomes an advantage, for it is what actually allows us to measure nematicity. Indeed, the orthorhombicity acts like the uniaxial pressure applied in the pioneer elastoresistivity experiments performed on iron-based superconductors [9], except that for YBCO, this pressure is internal and not external. However, the orthorhombic structure of YBCO comes with unidirectional CuO chains that run along the b axis of the crystal, and these chains are conductive. They therefore impose a background anisotropy in the

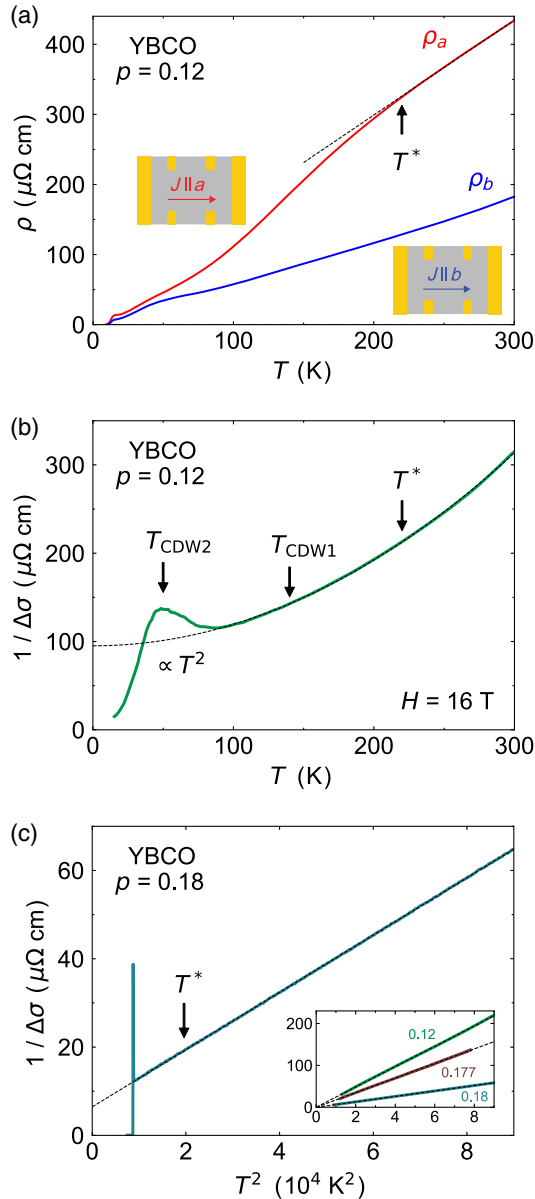


FIG. 2. In-plane resistivity of YBCO at $p = 0.12$, in a magnetic field of $H = 16$ T. (a) Temperature dependence of the resistivity along the a axis (ρ_a , red) and b axis (ρ_b , blue) of the orthorhombic crystal structure. T^* is defined as the departure in ρ_a from the T -linear dependence at high temperature (black dashed line). (This is called T_ρ in Fig. 1, but T^* hereafter.) A sketch of the sample and contacts is shown for each current direction. (b) Resistivity anisotropy, plotted as $1/\Delta\sigma = 1/(1/\rho_b - 1/\rho_a)$ versus T . The T^2 dependence of $1/\Delta\sigma$ (dashed line) coming from the CuO chains is seen to persist down to $T \approx 100$ K, showing that no nematicity develops below $T^* = 220$ K. The deviation below ≈ 100 K occurs inside the region of charge-density-wave ordering. (c) $1/\Delta\sigma$ versus T^2 of YBCO at $p = 0.18$ ($y = 6.998$) (from Ref. [16]). The CuO chains are fully oxygenated and maximally conductive at $p = 0.18$ and follow a T^2 dependence down to T_c . Inset: chain resistivity (with $T = 0$ value subtracted), at $p = 0.12$ (green, this work), $p = 0.177$ (violet, Ref. [16]), and $p = 0.18$ (blue, Ref. [16]). Dashed lines are T^2 fits.

transport properties that one needs to carefully take into account.

B. Samples

A single crystal of $\text{YBa}_2\text{Cu}_3\text{O}_y$ was prepared at the University of British Columbia by flux growth [22]. The detwinned sample is an uncut, unpolished thin platelet, with gold evaporated contacts (of resistance $< 1 \Omega$). Its hole concentration (doping) p is determined from the superconducting transition temperature T_c [23], defined as the temperature below which the zero-field resistance is zero. A high degree of oxygen order is achieved with $p = 0.12$ ($y = 6.67$, ortho-VIII order) and $T_c = 65.5$ K. To be able to compare with precision the measurements between the a - and b -axis directions, we have to get rid of the uncertainties associated with the geometric factors inherent to transport experiments—typically $\approx 15\%$ uncertainty because contacts have a certain width. To achieve this, the experiment is performed in a two-stage process. First, gold contacts are deposited on the surface of the sample in order to measure the a -axis transport coefficients [see Fig. 2(a)]. Then, the same sample with the same contacts is detwinned in the other crystallographic direction, which means a and b are rotated by 90° , allowing us to measure the b -axis transport coefficients with the same set of contacts.

C. Measurements

We measure the resistivity and Seebeck coefficient on the same YBCO $p = 0.12$ sample for a - and b -axis orientations of the crystal. Silver wires glued with silver paste on the gold contacts of the sample are used for both measurements. The electrical resistivity ρ is measured by sending an electric current along x and measuring the associated voltage difference along x , where x is first along the a axis and then along the b axis, using the exact same contacts. The Seebeck coefficient S is measured by sending a heat current along x and measuring the associated voltage difference and temperature difference along x , so that $S = \Delta V/\Delta T$, where again x is first along the a axis and then along the b axis. Note that a measurement of S involves two types of contacts—electrical and thermal—whose effective position along the length of the sample will in general be slightly different (although measured using the same gold pads), resulting in an uncertainty on S given roughly by contact width over contact separation, so about 10%. This introduces a small uncertainty on the Peltier coefficient α , which involves taking the ratio of S over ρ .

A magnetic field of 16 T is applied along the c axis, perpendicular to the CuO_2 planes, in order to partially suppress superconductivity and therefore extend the measurements to lower temperature.

III. RESULTS

To detect nematicity in YBCO, we measure the anisotropy of the resistivity and the Seebeck coefficient—two longitudinal probes of charge transport—between the a and b directions in our orthorhombic (monodomain) crystal.

A. Resistivity

In YBCO, the a -axis resistivity ρ_a reflects purely the conductivity of the CuO_2 planes; i.e., $1/\rho_a = \sigma_{\text{plane}}^a$. When the current is along b , however, there are two parallel channels of charge conduction: the two-dimensional CuO_2 planes (σ_{plane}^b) and the one-dimensional CuO chains (σ_{chain}), so that $1/\rho_b = \sigma_{\text{plane}}^b + \sigma_{\text{chain}}$. The large resulting anisotropy between ρ_a and ρ_b can clearly be seen in Fig. 2(a), in particular above T^* .

Fortunately, we can disentangle any anisotropy coming from the CuO_2 planes—as expected in the presence of nematicity—from the background anisotropy due to the CuO chains by using the fact that the chain resistivity follows a perfectly defined T^2 dependence from 300 K down to at least 90 K, as established by measurements in YBCO at high doping [16,24] and reproduced in Fig. 2(c). In Fig. 2(b), we examine the anisotropy of the conductivity, defined as the difference $\Delta\sigma = 1/\rho_b - 1/\rho_a$, by plotting our data as $1/\Delta\sigma$ versus T .

We observe that $1/\Delta\sigma$ follows a T^2 dependence down to $T \approx 100$ K, entirely coming from the CuO chains. The slope of the T^2 resistivity from the chains tends to decrease with increasing doping as shown in the inset of Fig. 2(c), as naively expected for CuO chains more and more conductive as $p \rightarrow 0.18$ when fully oxygenated. Although the resistivity of the CuO chains obeys a pristine T^2 dependence that remains to be theoretically understood, this allows us to subtract perfectly the chain contribution from the b -axis resistivity and access the pure anisotropy coming from the CuO_2 planes. The fact that no additional anisotropy in $1/\Delta\sigma$ is detected at $p = 0.12$ upon cooling below $T^* = 220$ K shows that the pseudogap phase causes no nematicity to emerge in the electron fluid. Note here that we cannot exclude that interchain conduction plays a role in the T^2 behavior of $1/\Delta\sigma$, and further investigation regarding the origin of the T^2 resistivity will be the subject of future work. However, we focus here on the absence of change in the T^2 dependence of the anisotropy in the resistivity at the pseudogap phase temperature onset, which does not require further hypothesis to conclude the absence of nematicity onset at T^* . In addition, this result is reproduced in the Appendix on two additional separate YBCO $p = 0.12$ samples.

Note, however, that there is a clear deviation from the T^2 background that occurs below 100 K or so [Fig. 2(a)]. We return to this feature in Sec. IV.

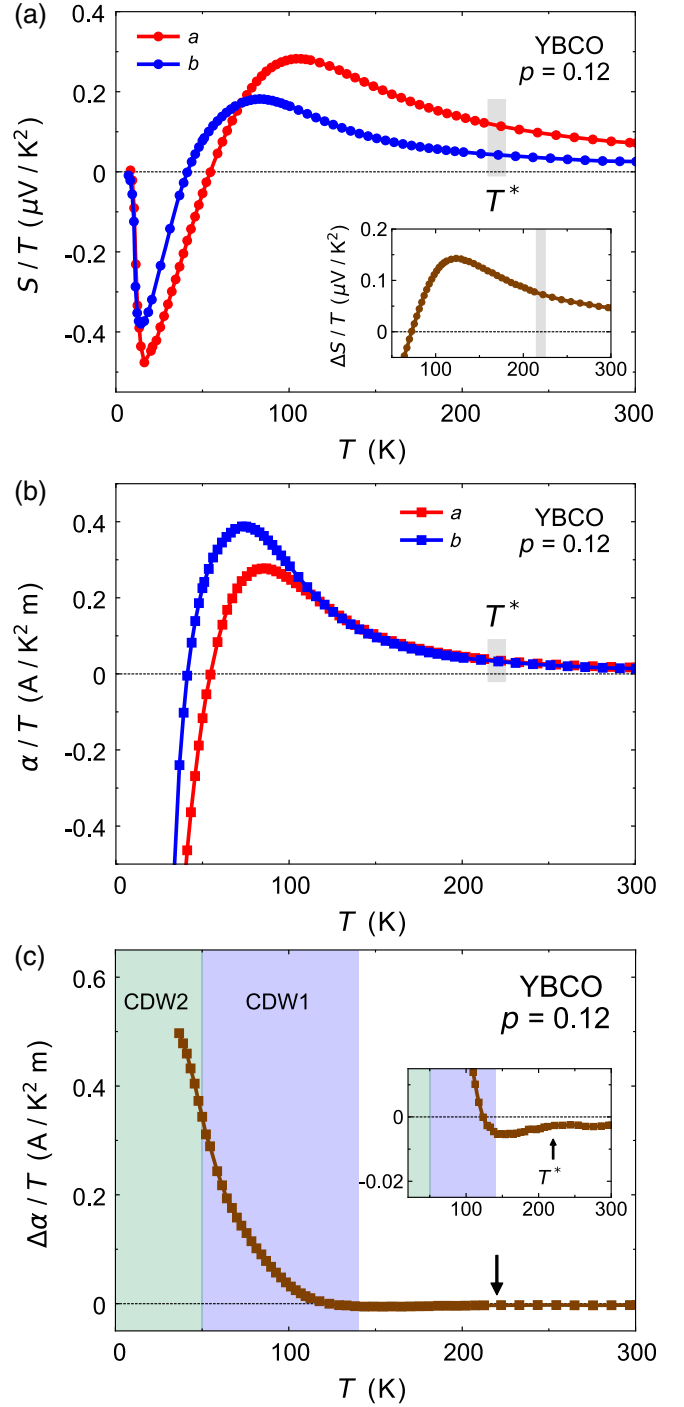


FIG. 3. Thermoelectric transport coefficient of YBCO at $p = 0.12$ in a magnetic field $H = 16$ T. (a) Temperature dependence of the Seebeck coefficient S along the a axis (red) and b axis (blue). The inset represents the difference $\Delta S/T = (S_a - S_b)/T$ versus T . T^* is marked by gray stripes. (b) Peltier coefficient $\alpha = S/\rho$ along a axis (red) and b axis (blue). T^* is marked by a gray stripe. (c) Anisotropy of the Peltier coefficient, plotted as $\Delta\alpha/T = (\alpha_b - \alpha_a)/T$ versus T . The arrow marks T^* . The blue shaded region indicates the regime of short-range two-dimensional charge-density-wave correlations and the green shaded region the regime of long-range three-dimensional charge-density-wave order. Inset: enlargement at high temperature.

B. Seebeck coefficient

To confirm our findings from resistivity, we measure the anisotropy of the Seebeck coefficient, another longitudinal coefficient. Our data are shown in Fig. 3(a), plotted as S/T versus T . A clear anisotropy is observed between S_a and S_b , even above T^* . In the inset, we plot the difference $\Delta S = S_a - S_b$, which does not show any anomaly at T^* . However, Seebeck is not an additive coefficient like the conductivity and we do not know what the background anisotropy from CuO chains should be in S . It makes this statement on the absence of nematicity at T^* less conclusive for the Seebeck coefficient than for the resistivity where the temperature dependence of the resistivity of CuO chains is known.

C. Peltier coefficient

To shed light on the anisotropy present in the Seebeck coefficient, we turn to the Peltier coefficient $\alpha = S/\rho$ —the fundamental thermoelectric transport coefficient. The advantage here is that α is additive while by definition S is not. In Fig. 3(b), we plot α/T versus T for both current directions. We see, strikingly, that α is almost isotropic down to $T \simeq 140$ K. The difference $\Delta\alpha = \alpha_a - \alpha_b = S_a/\rho_a - S_b/\rho_b$, plotted as $\Delta\alpha/T$ versus T in Fig. 3(c), is an order of magnitude smaller than the CuO₂ plane contribution, up to at least 300 K. The very small anisotropy in α above 140 K [inset of Fig. 3(c)], which amounts to $\Delta\alpha/\alpha \simeq 5\%$, reveals that CuO chains produce a very weak anisotropy in α . This experimental observation suggests that the electronic dispersion of the CuO chains is almost particle-hole symmetric, which remains to be understood.

This is convenient for our study of nematicity, because the background anisotropy from the CuO chains remains very small in the Peltier coefficient, which is not the case for the Seebeck coefficient whose relative anisotropy is an order of magnitude larger. So any additional anisotropy in α must be emerging spontaneously within the CuO₂ planes (although we cannot rule out the possibility that the chain response changes at the onset of the charge-density-wave order below 140 K). In Fig. 3(c), we see that no such spontaneous anisotropy occurs at T^* . So here again, now in the longitudinal Peltier coefficient, we detect no nematicity upon entry into the pseudogap phase. However, we do observe a large anisotropy below 100 K or so, which we discuss in the next section.

IV. DISCUSSION

A. Anisotropy in the Nernst coefficient

Our finding of no nematicity at T^* deduced separately from two longitudinal transport coefficients, ρ and α , seems to contradict the prior finding of nematicity at T^* reported by Daou *et al.* [16] deduced from the Nernst coefficient (a subset of the present authors published this earlier work). There is in fact no contradiction between the absence of

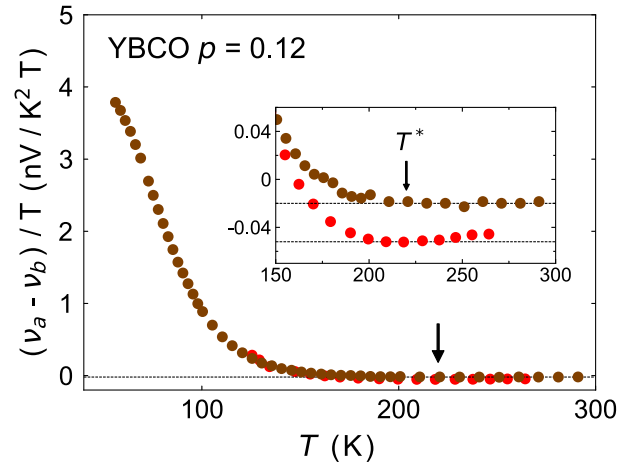


FIG. 4. Anisotropy in the Nernst coefficient ν , plotted as $(\nu_a - \nu_b)/T$ versus T for our YBCO $\rho = 0.12$ sample, at $H = 16$ T (full brown circles). Corresponding data reported by Daou *et al.* [16] are reproduced here in red. The inset shows that the rise in the Nernst anisotropy starts roughly at the same temperature T^* in the two studies.

anisotropy in the longitudinal coefficients and the presence of a small anisotropy in the Nernst coefficient. The apparent nematicity at T^* in the Nernst anisotropy is a small artifact of the composite nature of that coefficient. Indeed, as seen from Eq. (1), the Nernst anisotropy difference $(\nu_a - \nu_b)/T$ can in principle come from two terms, the first involving $(\alpha_a - \alpha_b)/T$ and the second involving $(\rho_a - \rho_b)$. While we now know that the first term is essentially zero between 300 and 140 K [Fig. 3(c)], the second term is nonzero, and it will change across $T^* = 220$ K, as can be seen by inspection of the resistivity data in Fig. 2(a). The Nernst coefficient will therefore pick up that slight change across T^* .

During the same two-stage experiment used to measure the anisotropy in the resistivity and the Seebeck coefficient, we also measured the Nernst coefficient. The resulting data are plotted in Fig. 4 as the difference $(\nu_a - \nu_b)/T$ versus T . These are consistent with the corresponding data reported by Daou *et al.* [16]. By enlarging the region at high temperature (inset), we see that the Nernst anisotropy starts to grow below $T \simeq 200$ K $\simeq T^*$. This growth is very slow, as by 140 K the Nernst anisotropy has only reached 1% of its full value at low temperature. It is this very slight additional anisotropy in $(\nu_a - \nu_b)/T$ versus T which led Daou *et al.* to conclude that nematicity starts at T^* . As we now know, it does not reflect any true nematicity.

B. Nematicity associated with CDW ordering

Of course, the 100-fold growth in the Nernst anisotropy that takes place between 150 and 50 K does reflect a true additional anisotropy, in a composite way. For a direct measure of nematicity, it is best to look at the Peltier anisotropy, because it is a longitudinal coefficient and it is

almost negligible at high temperature. In Fig. 3(c), we see that $(\alpha_b - \alpha_a)/T$ starts to rise below 140 K, and this growth is smooth and continuous down to at least 35 K. As done previously for the Nernst anisotropy [15], we attribute the emergence of the Peltier anisotropy to the development of charge-density-wave order. At $H = 16$ T, the charge ordering process is known from x-ray studies to occur in two stages [21,25–27]: first, short-range two-dimensional CDW correlations start to grow below $T_{\text{CDW1}} = 140 \pm 10$ K [20], then long-range three-dimensional charge order sets in at $T_{\text{CDW2}} = 47 \pm 1$ K [21]. The latter order is unidirectional, so it breaks rotational symmetry, as well as translational symmetry. It is clear from Fig. 3(c) that the growth in Peltier anisotropy occurs in tandem with the CDW ordering process. The same is true for the resistivity, whose anisotropy grows suddenly below ~ 100 K. This anisotropy can emerge from either an anisotropy in the carrier density or the scattering processes. If one considers that long-range translational symmetry is only broken at T_{CDW2} , then the region between T_{CDW2} and T_{CDW1} would be a nematic phase, where rotational symmetry is spontaneously broken in the electronic fluid of the CuO_2 planes, in agreement with NMR studies [28].

In summary, our controlled measurements of longitudinal transport conducted on a single YBCO sample for both current directions (a and b) allow us to show that previous signatures of nematicity based on Nernst measurements [15,16] do not onset at T^* , but at significantly lower temperature. Although we can only claim that electronic nematicity below T^* is unobservable within our resolution, the sharp signature reported at T^* in torque experiments [11] remains *a priori* incompatible with the absence of charge nematicity in longitudinal transport coefficients. Further investigations are needed to solve this apparent contradiction.

V. SUMMARY

We measured the in-plane anisotropy of the longitudinal charge transport coefficients of YBCO at a doping $p = 0.12$ —the resistivity and the Seebeck coefficient. Upon cooling through the pseudogap temperature T^* , we observe no additional in-plane anisotropy in the resistivity $\rho(T)$, beyond the background anisotropy due to the CuO chains, whose resistivity obeys a T^2 dependence that can therefore be readily subtracted. This shows that the pseudogap phase of cuprates is not nematic. Moreover, we find that the Peltier coefficient $\alpha = S/\rho$ remains almost isotropic across T^* , which confirms the absence of charge nematicity at the onset of the pseudogap phase.

However, a large anisotropy in the Peltier coefficient does develop at lower temperature in tandem with the growth in the short-range charge-density-wave correlations starting below $T_{\text{CDW1}} = 140$ K. This anisotropy continues to grow down to at least $T = 35$ K, below the onset of long-range charge-density-wave order at $T_{\text{CDW2}} = 47$ K

(in $H = 16$ T). Since translational symmetry is only truly broken, on a long length scale, at T_{CDW2} , we infer that the regime between T_{CDW2} and T_{CDW1} may be a nematic phase. In the absence of electronic nematicity at T^* , the anisotropy previously detected by torque magnetometry at T^* [11] must find a different origin.

ACKNOWLEDGMENTS

We thank S. Fortier for his assistance with the experiments. L. T. acknowledges support from the Canadian Institute for Advanced Research (CIFAR) as a CIFAR Fellow and funding from the Institut Quantique, the Natural Sciences and Engineering Research Council of Canada (PIN:123817), the Fonds de Recherche du Québec—Nature et Technologies (FRQNT), the Canada Foundation for Innovation (CFI), and a Canada Research Chair.

APPENDIX: DATA REPRODUCIBILITY

We carried out a measurement of $\rho_a(T)$ on a second YBCO sample (A) for which $J \parallel x \parallel a$ and a measurement of $\rho_b(T)$ on a third YBCO sample (B) for which $J \parallel x \parallel b$. All three samples come from the same source (University of British Columbia) and are prepared in such a way as to have very similar doping (as established by the T_c values). In Fig. 5, we display $\rho_a(T)$ and $\rho_b(T)$ for samples A and B. As can be seen, they are very similar to the curves reported in Fig. 2(a). However, there are small differences, which can come from the following three factors:

- (1) the uncertainty on the measurement of sample dimensions and contact separation, affecting the geometric factor used to obtain the resistivity from the resistance,
- (2) the degree of oxygen order within the CuO chains,
- (3) the density of impurities.

The advantage of our experiment on one and the same sample (to get both ρ_a and ρ_b) is that factor (1) above is eliminated and factors (2) and (3) are kept constant. This is

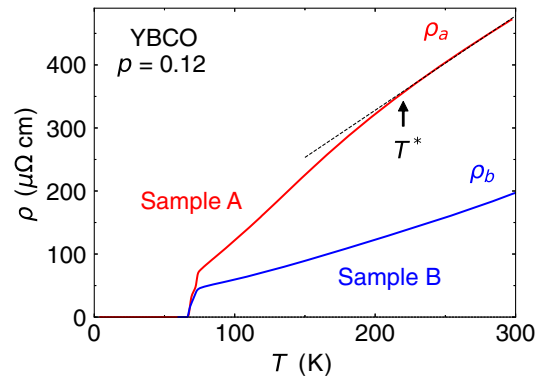


FIG. 5. Resistivity as a function of temperature for two additional samples of YBCO $p = 0.12$: sample A ($J \parallel a$) and sample B ($J \parallel b$), in zero magnetic field.

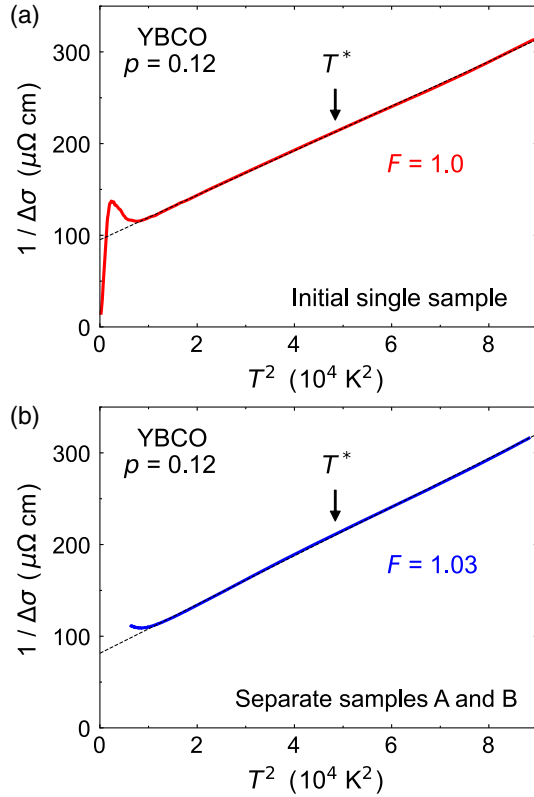


FIG. 6. $1/\Delta\sigma$ versus T^2 of YBCO at $p = 0.12$, using (a) the initial single sample of this study and (b) two separate samples A and B, with a factor F .

not the case when using two different samples, as for our pair of samples A and B.

In Fig. 6, we plot the quantity $1/\Delta\sigma$ versus T^2 , as done in Fig. 2(c), where $\Delta\sigma$ is defined as $\Delta\sigma = (F\sigma_b) - \sigma_a$. The factor F is a multiplicative factor that allows for the uncertainty on the sample dimensions [factor (1) above] and also, in a simplistic way, for the differences coming from factors (2) and (3) above. For Fig. 6(a), we use the data from the single sample reported in our article, with $F = 1.0$ [Fig. 2(b)]. For Fig. 6(b), we use the new data, namely $\sigma_a(T) = 1/\rho_a(T)$ from sample A and $\sigma_b(T) = 1/\rho_b(T)$ from sample B, and $F = 1.03$. This value of F is close enough to unity to be well within the error bars on sample dimensions, which are roughly $\pm 15\%$ for each sample.

We see that the new data, from two additional (and separate) samples of YBCO (with the same doping $p = 0.12$), yield a quadratic T dependence for $1/\Delta\sigma$ that is just as featureless and straight [Fig. 6(b)] as that reported for our initial single sample [Fig. 6(a) and Fig. 2]. In particular, there is no change in the anisotropy at the pseudogap temperature T^* .

We conclude that the main finding of our study is consistent, within error bars, with measurements on additional samples, confirming that there is no trace of nematicity appearing below T^* in the longitudinal charge conduction of YBCO.

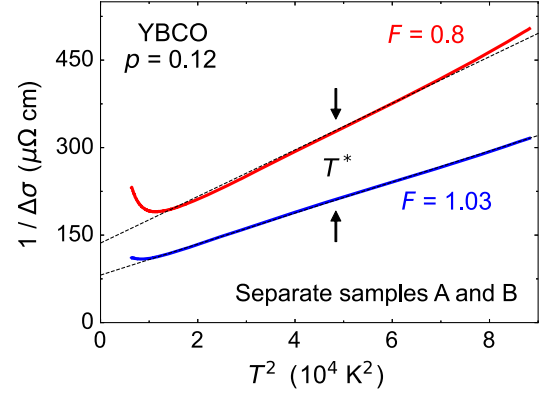


FIG. 7. $1/\Delta\sigma$ vs T^2 of YBCO at $p = 0.12$, using two separate samples, A and B, for two different values of F : $F = 1.03$ (blue) and $F = 0.8$ (red).

Note that using $F = 0.8$ —a value also consistent with error bars on sample dimensions—yields a T dependence for $1/\Delta\sigma$ which is not quadratic (Fig. 7), and as a result it is difficult to decide what anisotropy comes from the CuO chains and what anisotropy comes from the planes.

We see that in a two-sample study one must make the assumption that $1/\Delta\sigma$ should be quadratic—and adjust the geometric factors accordingly—in order to conclude that nothing happens at T^* . No such assumption is needed in our single-sample study.

-
- [1] B. Keimer, S. A. Kivelson, M. R. Norman, S. Uchida, and J. Zaanen, *From Quantum Matter to High-Temperature Superconductivity in Copper Oxides*, *Nature (London)* **518**, 179 (2015).
 - [2] C. Proust and L. Taillefer, *The Remarkable Underlying Ground States of Cuprate Superconductors*, *Annu. Rev. Condens. Matter Phys.* **10**, 409 (2019).
 - [3] O. Cyr-Choinière, R. Daou, F. Laliberté, C. Collignon, S. Badoux, D. LeBoeuf, J. Chang, B. J. Ramshaw, D. A. Bonn, W. N. Hardy *et al.*, *Pseudogap Temperature T^* of Cuprate Superconductors from the Nernst Effect*, *Phys. Rev. B* **97**, 064502 (2018).
 - [4] B. Fauqué, Y. Sidis, V. Hinkov, S. Pailhès, C. T. Lin, X. Chaud, and P. Bourges, *Magnetic Order in the Pseudogap Phase of High- T_c Superconductors*, *Phys. Rev. Lett.* **96**, 197001 (2006).
 - [5] J. Xia, E. Schemm, G. Deutscher, S. A. Kivelson, D. A. Bonn, W. N. Hardy, R. Liang, W. Siemons, G. Koster, M. M. Fejer, and A. Kapitulnik, *Polar Kerr-Effect Measurements of the High-Temperature $\text{YBa}_2\text{Cu}_3\text{O}_{6+x}$ Superconductor: Evidence for Broken Symmetry near the Pseudogap Temperature*, *Phys. Rev. Lett.* **100**, 127002 (2008).
 - [6] L. Zhao, C. A. Belvin, R. Liang, D. A. Bonn, W. N. Hardy, N. P. Armitage, and D. Hsieh, *A Global Inversion-Symmetry-Broken Phase inside the Pseudogap Region of $\text{YBa}_2\text{Cu}_3\text{O}_y$* , *Nat. Phys.* **13**, 250 (2016).

- [7] Y. Lubashevsky, L. D. Pan, T. Kirzhner, G. Koren, and N. P. Armitage, *Optical Birefringence and Dichroism of Cuprate Superconductors in the THz regime*, *Phys. Rev. Lett.* **112**, 147001 (2014).
- [8] M. J. Lawler, K. Fujita, J. Lee, A. R. Schmidt, Y. Kohsaka, C. K. Kim, H. Eisaki, S. Uchida, J. C. Davis, J. P. Sethna, and E.-A. Kim, *Intra-Unit-Cell Electronic Nematicity of the High- T_c Copper-Oxide Pseudogap States*, *Nature (London)* **466**, 347 (2010).
- [9] J.-H. Chu, H.-H. Kuo, J. G. Analytis, and I. R. Fisher, *Divergent Nematic Susceptibility in an Iron Arsenide Superconductor*, *Science* **337**, 710 (2012).
- [10] Y. Cao, D. Rodan-Legrain, J. M. Park, N. F. Q. Yuan, K. Watanabe, T. Taniguchi, R. M. Fernandes, L. Fu, and P. Jarillo-Herrero, *Nematicity and Competing Orders in Superconducting Magic-Angle Graphene*, *Science* **372**, 264 (2021).
- [11] Y. Sato, S. Kasahara, H. Murayama, Y. Kasahara, E.-G. Moon, T. Nishizaki, T. Loew, J. Porras, B. Keimer, T. Shibauchi, and Y. Matsuda, *Thermodynamic Evidence for a Nematic Phase Transition at the Onset of the Pseudogap in $\text{YBa}_2\text{Cu}_3\text{O}_y$* , *Nat. Phys.* **13**, 1074 (2017).
- [12] Y. Ando, S. Komiya, K. Segawa, S. Ono, and Y. Kurita, *Electronic Phase Diagram of High- T_c Cuprate Superconductors from a Mapping of the In-Plane Resistivity Curvature*, *Phys. Rev. Lett.* **93**, 267001 (2004).
- [13] Y. Ando, K. Segawa, S. Komiya, and A. N. Lavrov, *Electrical Resistivity Anisotropy from Self-Organized One Dimensionality in High-Temperature Superconductors*, *Phys. Rev. Lett.* **88**, 137005 (2002).
- [14] V. Hinkov, P. Bourges, S. Pailhès, Y. Sidis, A. Ivanov, C. D. Frost, T. G. Perring, C. T. Lin, D. P. Chen, and B. Keimer, *Spin Dynamics in the Pseudogap State of a High-Temperature Superconductor*, *Nat. Phys.* **3**, 780 (2007).
- [15] O. Cyr-Choinière, G. Grissonnanche, S. Badoux, J. Day, D. A. Bonn, W. N. Hardy, R. Liang, N. Doiron-Leyraud, and L. Taillefer, *Two Types of Nematicity in the Phase Diagram of the Cuprate Superconductor $\text{YBa}_2\text{Cu}_3\text{O}_y$* , *Phys. Rev. B* **92**, 224502 (2015).
- [16] R. Daou, J. Chang, D. LeBoeuf, O. Cyr-Choinière, F. Laliberté, N. Doiron-Leyraud, B. J. Ramshaw, R. Liang, D. A. Bonn, W. N. Hardy, and L. Taillefer, *Broken Rotational Symmetry in the Pseudogap Phase of a High- T_c Superconductor*, *Nature (London)* **463**, 519 (2010).
- [17] K. Ishida, S. Hosoi, Y. Teramoto, T. Usui, Y. Mizukami, K. Itaka, Y. Matsuda, T. Watanabe, and T. Shibauchi, *Divergent Nematic Susceptibility near the Pseudogap Critical Point in a Cuprate Superconductor*, *J. Phys. Soc. Jpn.* **89**, 064707 (2020).
- [18] T. A. Maier and D. J. Scalapino, *Pairing Interaction near a Nematic Quantum Critical Point of a Three-Band CuO_2 Model*, *Phys. Rev. B* **90**, 174510 (2014).
- [19] S. Lederer, Y. Schattner, E. Berg, and S. A. Kivelson, *Enhancement of Superconductivity near a Nematic Quantum Critical Point*, *Phys. Rev. Lett.* **114**, 097001 (2015).
- [20] J. Chang, E. Blackburn, A. T. Holmes, N. B. Christensen, J. Larsen, J. Mesot, R. Liang, D. A. Bonn, W. N. Hardy, A. Watenphul, M. v. Zimmermann, E. M. Forgan, and S. M. Hayden, *Direct Observation of Competition between Superconductivity and Charge Density Wave Order in $\text{YBa}_2\text{Cu}_3\text{O}_{6.67}$* , *Nat. Phys.* **8**, 871 (2012).
- [21] J. Chang, E. Blackburn, O. Ivashko, A. T. Holmes, N. B. Christensen, M. Hücker, R. Liang, D. A. Bonn, W. N. Hardy, U. Rütt, M. v. Zimmermann, E. M. Forgan, and S. M. Hayden, *Magnetic Field Controlled Charge Density Wave Coupling in Underdoped $\text{YBa}_2\text{Cu}_3\text{O}_{6+x}$* , *Nat. Commun.* **7**, 1 (2016).
- [22] R. Liang, D. A. Bonn, and W. N. Hardy, *Growth of YBCO Single Crystals by the Self-Flux Technique*, *Philos. Mag.* **92**, 2563 (2012).
- [23] R. Liang, D. A. Bonn, and W. N. Hardy, *Evaluation of CuO_2 Plane Hole Doping in $\text{YBa}_2\text{Cu}_3\text{O}_{6+x}$ Single Crystals*, *Phys. Rev. B* **73**, 180505(R) (2006).
- [24] R. Gagnon, C. Lupien, and L. Taillefer, *T^2 Dependence of the Resistivity in the Cu-O Chains of $\text{YBa}_2\text{Cu}_3\text{O}_{6.9}$* , *Phys. Rev. B* **50**, 3458 (1994).
- [25] M. Hücker, N. B. Christensen, A. T. Holmes, E. Blackburn, E. M. Forgan, R. Liang, D. A. Bonn, W. N. Hardy, O. Gutowski, M. v. Zimmermann, S. M. Hayden, and J. Chang, *Competing Charge, Spin, and Superconducting Orders in Underdoped $\text{YBa}_2\text{Cu}_3\text{O}_y$* , *Phys. Rev. B* **90**, 054514 (2014).
- [26] S. Blanco-Canosa, A. Frano, E. Schierle, J. Porras, T. Loew, M. Minola, M. Bluschke, E. Weschke, B. Keimer, and M. Le Tacon, *Resonant X-Ray Scattering Study of Charge-Density Wave Correlations in $\text{YBa}_2\text{Cu}_3\text{O}_{6+x}$* , *Phys. Rev. B* **90**, 054513 (2014).
- [27] S. Gerber, H. Jang, H. Nojiri, S. Matsuzawa, H. Yasumura, D. A. Bonn, R. Liang, W. N. Hardy, Z. Islam, A. Mehta *et al.*, *Three-Dimensional Charge Density Wave Order in $\text{YBa}_2\text{Cu}_3\text{O}_{6.67}$ at High Magnetic Fields*, *Science* **350**, 949 (2015).
- [28] T. Wu, H. Mayaffre, S. Krämer, M. Horvatić, C. Berthier, W. N. Hardy, R. Liang, D. A. Bonn, and M.-H. Julien, *Incipient Charge Order Observed by NMR in the Normal State of $\text{YBa}_2\text{Cu}_3\text{O}_y$* , *Nat. Commun.* **6**, 6438 (2015).